Structure of the $^3H \rightarrow n+d(d^*)$ vertexes

B. F. Gibson
Theoretical Division, Los Alamos National Laboratory, Los Alamos, New Mexico 87545

D. R. Lehman
Department of Physics, The George Washington University, Washington, D. C. 20052
(Received 17 October 1983)

Models of ^3H are constructed from $^1S_0$ and $^3S_1$-$^3D_1$ separable interactions fitted to low-energy two-nucleon properties. In particular, a set of $^3S_1$-$^3D_1$ interactions is used that produces D-wave components in the deuteron with $P_D = 0\%$ to 10%. The ^3H binding energy (B_3), ^3H wave-function component percentages, $^3H \rightarrow n+d(d^*)$ asymptotic normalization constants, $^3H \rightarrow n+d$ distorted wave parameters, percentage n-d component in the ^3H wave function, and $^3H \rightarrow n+d$ momentum distribution are calculated for each case. From these results, numerous aspects of the $^3H \rightarrow n+d(d^*)$ vertexes are examined. As examples: (1) dependence of the S- and D-wave $^3H \rightarrow n+d$ asymptotic norms on P_D and B_3; (2) dependence of the $^3H \rightarrow n+d^*$ asymptotic norm on the scattering length and effective range of the $^1S_0$ interaction; (3) role of the D-wave component of the $^3H \rightarrow n+d$ momentum distribution for n-d relative momentum between 0 and 2 fm^{-1}; and (4) validity of approximating the $^3H \rightarrow n+d$ distorted-wave parameter, D_2, by the ratio of the D- to S-wave asymptotic normalization constants. Where possible, comparisons are made with local-potential calculations and experiment.

[NUCLEAR STRUCTURE Faddeev calculations. $^3H \rightarrow n+d$ or $^3H \rightarrow n+d^*$ vertex structure. Deuteron D-wave effects on ^3H vertex structure.]

I. INTRODUCTION

Elastic scattering of electrons or protons from the trinucleons (^3H or ^3He) yields information on the convolution of the trinucleon ground-state wave function with itself. For example, elastic electron scattering permits extraction of the charge and magnetic form factors.[1,2] On the other hand, inelastic scattering of electrons or protons from the trinucleons, especially coincidence experiments like $^3He(e,e'p)d$, $^3He(e,e'p)np$, $^3He(p,pd)n$, etc., yields information on the overlap between the trinucleon ground-state wave function and the wave function of a nucleon moving freely relative to a deuteron or the wave function of a nucleon moving freely relative to a pair of nucleons in a scattering state.[3] Knowledge of the latter two types of overlap is important, because these overlaps, evaluated as a function of the relative momentum of the freely moving nucleon with respect to the center of mass of the interacting pair, give the structure of the trinucleon vertexes $^3H \rightarrow n+d$, $^3H \rightarrow n+d^*$, $^3He \rightarrow p+d$, and so on. This structural information comes in the form of momentum distributions, asymptotic normalization constants, distorted-wave parameters (D_l), and related quantities. Now that recent experiments permit the extraction of such properties[3,4] and that the three-body theory is at a state where calculations[4] can be made with the best available two-nucleon interactions, it is worthwhile to examine how the theoretical results depend on certain underlying two-nucleon properties.

The objectives of this work are twofold: (1) determine the dependence of the structural quantities for the $^3H \rightarrow n+d$ vertex on the percentage D-state component (P_D) in the deuteron wave function, and (2) determine the sensitivity of the $^3H \rightarrow n+d^*$ asymptotic norm[5] to the underlying two-nucleon, spin-singlet scattering length and effective range. These investigations are carried through by means of separable-potential models where it is possible to vary one aspect of the underlying two-nucleon properties while keeping other aspects fixed. Nevertheless, we shall see that such simple models make essentially the same predictions for the observables under consideration as do sophisticated two-nucleon models like the Reid soft-core potential,[6] when the separable models have the same low-energy properties. This emphasizes the role that simple models play in better understanding three-nucleon properties, as long as the simple models are used within their domain of applicability. The vertex structural information considered in this work primarily involves the asymptotic and longer-range side of the intermediate-range regions of the trinucleon wave functions. For this reason, separable models without two-nucleon, short-range repulsion are reasonable. The critical input is the low-energy s-wave two-nucleon scattering parameters and the tensor force as specified by both the deuteron quadrupole moment and the choice of P_D. The latter quantity, P_D, is our central focus with respect to the $^3H \rightarrow n+d$ vertex.

Though P_D is not a measurable quantity,[7] it is a characteristic parameter of the $^3S_1$-$^3D_1$ two-nucleon interaction, and as such, plays a role in the nature of the predictions concerning the $^3\mathrm{H}\rightarrow\mathrm{n}+\mathrm{d}$ vertex.

The format of the paper is as follows: In Sec. II, the formalism for obtaining the properties of the $^3\mathrm{H}\rightarrow\mathrm{n}+\mathrm{d}(\mathrm{d}^*)$ vertexes is presented; first for $^3\mathrm{H}\rightarrow\mathrm{n}+\mathrm{d}$ and then for $^3\mathrm{H}\rightarrow\mathrm{n}+\mathrm{d}^*$. The models employed are explained in Sec. III, followed in the same section with the numerical results. The results for the asymptotic normalization constants, momentum distributions, and distorted-wave parameters are discussed in Sec. IV. The main body of the paper closes with Sec. V, where the key conclusions are summarized. Two appendices complete the text: one concerns the structure of the three-body wave functions and the other discusses a singularity that must be handled carefully in calculating the singlet asymptotic norm.

II. FORMALISM

A. $^3\mathrm{H}\rightarrow\mathrm{n}+\mathrm{d}$ vertex

The key element in calculating the structure of the $^3\mathrm{H}\rightarrow\mathrm{n}+\mathrm{d}$ vertex is the amplitude obtained by overlapping the $^3\mathrm{H}$ ground-state wave function given in Appendix A with a wave function for a neutron of relative momentum $\vec{\mathrm{q}}$ moving freely relative to a deuteron. With the deuteron wave function written as ($\gamma^2=MB_2$)

$$\psi_m^{[1]}(\vec{\mathrm{p}})=N_\mathrm{d}\sqrt{4\pi}\sum_{l=0,2}\frac{g_l^1(p)}{p^2+\gamma^2}\times[Y^{[l]}(\hat{p})\times\chi^{[1]}(12)]_m^{[1]}\,, \tag{1}$$

this amplitude has the form ($\mathscr{A}\equiv$ antisymmetrized states)

$$\mathscr{A}\langle\mathrm{nd};\vec{\mathrm{q}},\tfrac{1}{2}m_\mathrm{n}1m_\mathrm{d}\,|\,^3\mathrm{H};\tfrac{1}{2}m_\mathrm{H}\rangle=\tfrac{3}{2}\sum_{\substack{l=0,2\\ m_l}}\sum_{\substack{J=1/2,3/2\\ M_J}}f_l(q)\langle\tfrac{1}{2}m_\mathrm{n}1m_\mathrm{d}\,|\,JM_J\rangle\langle lm_lJM_J\,|\,\tfrac{1}{2}m_\mathrm{H}\rangle\sqrt{4\pi}Y_{m_l}^{[l]}(\hat{q})\,, \tag{2}$$

where the isospin quantum numbers are suppressed. The momentum-distribution amplitudes are defined as follows:

$$f_0(q)=\mathrm{NN_d}\left\{a_0^1(q)4\pi\int_0^\infty k^2dk\frac{\sum_{l=0,2}[g_l^1(k)]^2}{(k^2+\gamma^2)\left[k^2+\frac{3q^2}{4}+K^2\right]}\right.$$
$$\left.+\pi\int_0^\infty k^2dk[-3\,{}_0^1\mathscr{I}_0^0(q,k;K^2)a_0^0(k)+{}_0^1\mathscr{I}_0^1(q,k;K^2)a_0^1(k)-{}_0^1\mathscr{I}_2^1(q,k;K^2)a_2^1(k)]\right\} \tag{3}$$

and

$$f_2(q)=\mathrm{NN_d}\left\{a_2^1(q)4\pi\int_0^\infty k^2dk\frac{\sum_{l=0,2}[g_l^1(k)]^2}{(k^2+\gamma^2)\left[k^2+\frac{3q^2}{4}+K^2\right]}\right.$$
$$\left.+\pi\int_0^\infty k^2dk[3\,{}_2^1\mathscr{I}_0^0(q,k;K^2)a_0^0(k)-{}_2^1\mathscr{I}_0^1(q,k;K^2)a_0^1(k)+{}_2^1\mathscr{I}_2^1(q,k;K^2)a_2^1(k)]\right\}. \tag{4}$$

All quantities appearing in Eqs. (3) and (4) are defined in Appendix A, except for the ${}_l^S\mathscr{I}_{l'}^{S'}$; however, the ${}_l^S\mathscr{I}_{l'}^{S'}$ are identical to the ${}_l^SI_{l'}^{S'}$ in Appendix A if $\Delta(k,p,x;K^2)\rightarrow\mathscr{D}(k,p,x;K^2)$, where

$$\mathscr{D}(k,p,x;K^2)=\left[k^2+\frac{p^2}{4}+\gamma^2+kpx\right]\times(k^2+p^2+K^2+kpx)\,. \tag{5}$$

The S- and D-wave $^3\mathrm{H}\rightarrow\mathrm{n}+\mathrm{d}$ momentum distribution amplitudes play a central role in calculations of the $^3\mathrm{H}\rightarrow\mathrm{n}+\mathrm{d}$ momentum distribution, the S- and D-wave asymptotic normalization constants, and the percentage n-d component in the $^3\mathrm{H}$ wave function.

The $^3\mathrm{H}\rightarrow\mathrm{n}+\mathrm{d}$ momentum distribution can be extracted from ^{3}He(p,2p)d or ^{3}He(e,e'p)d experiments (assuming isospin invariance) when the incident projectile has sufficient energy to minimize distortion effects, plus the eject-

ed particle comes out with sufficient energy to assure it was the particle that interacted with the projectile, i.e., essentially quasifree kinematics. These conditions can be satisfied with projectiles having $\gtrsim 300$ MeV kinetic energy. Such conditions permit analysis of the data (within 10% or so) on the basis of pole dominance as shown in Fig. 1. For either reaction, the general form of the coincidence cross section is[8]

$$\frac{d^3\sigma}{d\Omega_i d\epsilon_i d\Omega_p} = \frac{d\sigma}{d\Omega_{ip}}(\mathrm{kf})\tfrac{3}{2}\{[f_0(q)]^2+2[f_2(q)]^2\} , \quad (6)$$

where $i =$ e or p, $d\sigma/d\Omega_{ip}$ is the "half-off-shell" i-p scattering cross section, (kf) represents a kinematic factor, and $\frac{3}{2}\{\cdots\}$ is the momentum distribution. It is such a momentum distribution that has recently been extracted from the ^{3}He(e,e'p)d experiment at Saclay[3] and it can serve as a test of our model.

The integral d^3q over the quantity in the brackets $\{\cdots\}$ of Eq. (6) is usually called the spectroscopic factor. Closely related to the spectroscopic factor is the fraction of the neutron-deuteron component in the ^{3}H wave function. This quantity, denoted by P_{nd}, is given by

$$P_{nd} = 2\pi \int_0^\infty q^2 dq\{[f_0(q)]^2+[f_2(q)]^2\} , \quad (7)$$

which follows directly from the completeness relation

$$\sum_{m_S m_I}\sum_{SM_S IM_I}\int d^3q\, d^3k \mid N(\mathrm{NN})^{SI}_{\vec{k}};\vec{q}\,\tfrac{1}{2}m_S SM_S;\tfrac{1}{2}m_I IM_I\rangle \times\langle N(\mathrm{NN})^{SI}_{\vec{k}};\vec{q}\,\tfrac{1}{2}m_S SM_S;\tfrac{1}{2}m_I IM_I \mid = 1 . \quad (8)$$

The neutron-deuteron term of the completeness equation, i.e.,

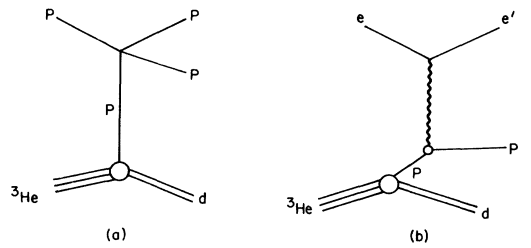

FIG. 1. Pole dominance graphs containing the common vertex $^3\mathrm{He}\rightarrow \mathrm{p}+\mathrm{d}$. (a) ^{3}He(p,2p)d, (b) ^{3}He(e,e'p)d.

$$\sum_{m_S M_S}\int d^3q \mid n(\mathrm{np})^{10}_{\mathrm{d}};\vec{q}\,\tfrac{1}{2}m_S 1M_S;\tfrac{1}{2}-\tfrac{1}{2}00\rangle \times\langle n(\mathrm{np})^{10}_{\mathrm{d}};\vec{q}\,\tfrac{1}{2}m_S 1M_S;\tfrac{1}{2}-\tfrac{1}{2}00 \mid ,$$

inserted in the normalization equation for the ^{3}H state vector,

$$\tfrac{1}{2}\sum_{m_H}\langle {}^3\mathrm{H};\tfrac{1}{2}m_H \mid {}^3\mathrm{H};\tfrac{1}{2}m_H\rangle = 1 , \quad (9)$$

yields P_{nd}. The factor 2π instead of 4π in front of the integral arises from the fact that the states in the completeness relation are not antisymmetrized. Thus, the $\sqrt{3}$ appearing in Eq. (2) is absent, but the $1/\sqrt{2}$ remains and the spin sums lead to $\frac{1}{2}\{[f_0(q)]^2+[f_2(q)]^2\}$.

Correspondingly, an effective neutron-deuteron wave function can be defined by means of the Fourier transform of Eq. (2), when the neutron-deuteron state is not antisymmetrized ($\sqrt{3}$ absent). With the coordinate $\vec{\rho}$ conjugate to $\vec{q}$, we define

$$\langle \mathrm{nd};\vec{\rho},\tfrac{1}{2}m_n 1m_d \mid {}^3\mathrm{H};\tfrac{1}{2}m_H\rangle = \sum_{\substack{l=0,2\\ m_l}}\sum_{\substack{J=1/2,3/2\\ M_J}} i^l u_l(\rho)\langle \tfrac{1}{2}m_n 1m_d \mid JM_J\rangle\langle lm_l JM_J \mid \tfrac{1}{2}m_H\rangle\sqrt{4\pi}\,Y^{[l]}_{m_l}(\hat{\rho}) , \quad (10)$$

where

$$u_l(\rho) = \frac{1}{\sqrt{\pi}}\int_0^\infty q^2 dq\, j_l(\rho q) f_l(q) . \quad (11)$$

In terms of the effective neutron-deuteron wave function, Eq. (7) becomes

$$P_{nd} = 4\pi \int_0^\infty \rho^2 d\rho\{[u_0(\rho)]^2+[u_2(\rho)]^2\} . \quad (12)$$

Consistent with the configuration-space version of the ^{3}H wave function given in Appendix A, the S- and D-wave $^3\mathrm{H}\rightarrow \mathrm{n}+\mathrm{d}$ asymptotic normalization constants, C_l^S, can be defined by means of the $u_l(\rho)$:

$$\lim_{\rho\rightarrow\infty} u_0(\rho) \rightarrow C_S^1\sqrt{\mu/2\pi}\frac{e^{-\mu\rho}}{\rho}\frac{1}{\sqrt{2}} \quad (13)$$

and

$$\lim_{\rho\rightarrow\infty} u_2(\rho) \rightarrow C_D^1\sqrt{\mu/2\pi}\frac{e^{-\mu\rho}}{\rho}\left[1+\frac{3}{\mu\rho}+\frac{3}{\mu^2\rho^2}\right]\frac{1}{\sqrt{2}} , \quad (14)$$

where $\mu^2 = 4(K^2-\gamma^2)/3$. The $1/\sqrt{2}$ at the right of each expression is associated with the isospin:

$$\lim_{\rho\to\infty}\Psi^{[1/2]}(\vec{r},\vec{\rho})\to C_S^1\sqrt{\mu/2\pi}\frac{e^{-\mu\rho}}{\rho}\sqrt{4\pi}[[Y^{[0]}(\hat{\rho})\times\chi^{[1/2]}(1)]^{[1/2]}\times\Phi_d^{[1]}(\vec{r})]^{[1/2]}\frac{\eta'}{\sqrt{2}}$$
$$-C_D^1\sqrt{\mu/2\pi}\frac{e^{-\mu\rho}}{\rho}\left[1+\frac{3}{\mu\rho}+\frac{3}{\mu^2\rho^2}\right]\sqrt{4\pi}[[Y^{[2]}(\hat{\rho})\times\chi^{[1/2]}(1)]^{[3/2]}\times\Phi_d^{[1]}(\vec{r})]^{[1/2]}\frac{\eta'}{\sqrt{2}}\ . \quad (15)$$

Integral relations for the C_l^1 can be derived by means of

$$\lim_{\rho\to\infty}u_l(\rho)=\frac{1}{\sqrt{\pi}}\lim_{\rho\to\infty}\int_0^\infty q^2dq\,j_l(\rho q)f_l(q)\ , \quad (16)$$

and the singularity structure of the $f_l(q)$ as given by Eqs. (3), (4), (A20), and (A21). The singularity in the $f_l(q)$ that leads to the dominant asymptotic behavior of the $u_l(\rho)$ comes from the $a_l^1(q)$, and it is a pole at $q=i\mu$. Specifically, we derive

$$C_l^1=i^l\left[2\pi i\mu^{1/2}\lim_{q\to i\mu}(q-i\mu)f_l(q)\right]\ , \quad (17)$$

so that

$$C_S^1=\frac{4\pi^2NN_d}{3\mu^{1/2}}\int_0^\infty k^2dk[-3_0^1I_0^0(i\mu,k;K^2)a_0^0(k)$$
$$+{}_0^1I_0^1(i\mu,k;K^2)a_0^1(k)$$
$$-{}_0^1I_2^1(i\mu,k;K^2)a_2^1(k)] \quad (18)$$

and

$$C_D^1=-\frac{4\pi^2NN_d}{3\mu^{1/2}}\int_0^\infty k^2dk[3_2^1I_0^0(i\mu,k;K^2)a_0^0(k)$$
$$-{}_2^1I_0^1(i\mu,k;K^2)a_0^1(k)$$
$$+{}_2^1I_2^1(i\mu,k;K^2)a_2^1(k)]\ . \quad (19)$$

Besides the asymptotic normalization constants, there are the related distorted-wave (DW) parameters D_0 and D_2. The DW parameters[4,9] are obtained from the $f_l(q)$ at $q=0$ ($K^2=MB_3$):

$$D_0=2\pi^{3/2}(B_3-B_2)f_0(0) \quad (20)$$

and

$$D_2=\lim_{q\to0}\left[\frac{-f_2(q)}{q^2f_0(q)}\right]\ . \quad (21)$$

By inverting Eq. (11), Eq. (21) can be written as

$$D_2=-\frac{\int_0^\infty\rho^4d\rho\,u_2(\rho)}{15\int_0^\infty\rho^2d\rho\,u_0(\rho)}\ . \quad (22)$$

To the extent that the main contribution to the integrals in Eq. (22) comes from the region of large ρ in the limit that $q\to0$, we can replace the $u_l(\rho)$ by their asymptotic forms from Eqs. (13) and (14), and then derive an *approximate* relationship between D_2 and the C_l^1:

$$D_2\cong-\frac{C_D^1}{\mu^2C_S^1}\equiv\tilde{D}_2\ . \quad (23)$$

We shall check the validity of this approximation with the models discussed below.

B. $^3H\to n+d^*$ vertex

The quantity on which we concentrate with respect to the $^3H\to n+d^*$ vertex is the $^3H\to n+d^*$ asymptotic normalization constant, a quantity that apparently will be difficult to extract from experiment but that carries useful information about the ^3H vertex structure. In this subsection, we derive an integral relation for the $^3H\to n+d^*$ asymptotic normalization, C_S^0, similar to the one given for C_S^1 in Eq. (18) above. The approach follows that of Harper, Lehman, and Prats.[5]

In dealing with the structure of the $^3H\to n+d$ vertex, the deuteron-^3H overlap is easily calculated, because the deuteron wave function is normalizable. This is not the case for the virtual-bound-state ($^1S_0$), d^*. Nevertheless, an alternative procedure for deriving C_S^1 leads to a straightforward method for deriving C_S^0. The key is to observe that (assuming s-wave NN interactions for clarity)

$$C_S^1=\frac{(2\pi)^2\sqrt{\mu\gamma}}{C_S^d}\lim_{q\to i\mu}(q-i\mu)$$
$$\times\lim_{k\to i\gamma}(k-i\gamma)\langle\phi_{\vec{k}}^{(-)^{10}};\vec{q}\alpha\,|\,\Psi\rangle \quad (24)$$

is an equivalent way of defining C_S^1. Here $\phi_{\vec{k}}^{(-)^{10}}$ is the spin-1, isospin-0 two-nucleon scattering state, C_S^d is the deuteron asymptotic normalization constant expressible in terms of the triplet effective range as $(1-\gamma r_{0_t})^{-1/2}$, α represents suppressed spin-isospin quantum numbers, and Ψ is the ^3H state vector. This method of defining C_S^1 follows from

$$\lim_{k\to i\gamma}(k-i\gamma)\langle\phi_{\vec{k}}^{(-)^{10}};\vec{q}\alpha\,|\,\Psi\rangle=\lim_{k\to i\gamma}(k-i\gamma)\langle\vec{k};\vec{q}\alpha\,|\,\Psi\rangle-\lim_{k\to i\gamma}(k-i\gamma)\langle\vec{k};\vec{q}\alpha\,|\,t^{10}\left[E^+-\frac{3q^3}{4M}\right]G_0(E^+)\,|\,\Psi\rangle\ , \quad (25)$$

where G_0 is the free three-nucleon resolvent, t^{10} is the two-nucleon t matrix, and $E^+ = k^2/M + 3q^2/4M + i\eta$. The first term on the right-hand side of Eq. (25) vanishes, whereas the second term leads to the deuteron wave function overlap

$$\lim_{k \to i\gamma} (k - i\gamma) \langle \phi^{(-)^{10}}_{\vec{k}}; \vec{q}\alpha \mid \Psi \rangle = -\frac{C_S^d}{2\pi i \gamma^{1/2}} \langle \phi_d; \vec{q}\alpha \mid \Psi \rangle \ . \tag{26}$$

Combining Eqs. (24) and (26), we get

$$C_S^1 = 2\pi i \mu^{1/2} \lim_{q \to i\mu} (q - i\mu) \langle \phi_d; \vec{q}\alpha \mid \Psi \rangle \ , \tag{27}$$

which is equivalent to Eq. (17).

Analogously, C_S^0 can be defined as follows:

$$C_S^0 = \frac{(2\pi)^2 \sqrt{-\mu^* \gamma^*}}{C_{d^*}} \lim_{q \to i\mu^*} (q - i\mu^*) \times \lim_{k \to -i\gamma^*} (k + i\gamma^*) \langle \phi^{(-)^{01}}_{\vec{k}}; \vec{q}\alpha \mid \Psi \rangle \ , \tag{28}$$

where $\mu^{*2} = 4M(B_3 - \gamma^{*2}/M)/3$, $C_{d^*} \cong (1 + \gamma^* r_{0_s})^{-1/2}$, and γ^* determines the location of the virtual bound-state pole possessed by the two-nucleon spin-0, isospin-1 t matrix which appears on the second sheet of the complex energy plane; i.e., $E_{\text{pole}} = -\gamma^{*2}/M$ on the negative real axis of the second sheet. Straightforward algebra leads to

$$C_S^0 = 2\pi i \mu^* \lim_{q \to i\mu^*} (q - i\mu^*) \langle \phi_{d^*}; \vec{q}\alpha \mid \Psi \rangle \ , \tag{29}$$

where, in momentum space,

$$\phi_{d^*}(p) = \frac{2\pi i (-\gamma^*)^{1/2} M}{C_{d^*}} \frac{\lim_{k \to -i\gamma^*} (k + i\gamma^*) \langle \vec{p} \mid t^{01}(E_k^+) \mid \vec{k} \rangle}{p^2 + \gamma^{*2}} \tag{30}$$

and $E_k^+ = k^2/M + i\eta$. Specifically, for the separable potentials of the present work, the last equation yields

$$\phi_{d^*}(p) = \left[\frac{-\beta_0^0 \gamma^* (\beta_0^0 - \gamma^*)^3}{\pi^2} \right]^{1/2} \frac{g_0^0(p)}{p^2 + \gamma^{*2}} \tag{31}$$

$$\equiv \frac{N_{d^*} g_0^0(p)}{p^2 + \gamma^{*2}} \ . \tag{32}$$

Thus, the sought-after formula emerges as

$$C_S^0 = \frac{4\pi^2 N N_{d^*}}{3\mu^{*1/2}} \int_0^\infty k^2 dk [{}_0^0 I_0^0(i\mu^*, k; K^2) a_0^0(k) - 3_0^0 I_0^1(i\mu^*, k; K^2) a_0^1(k) + 3_0^0 I_2^1(i\mu^*, k; K^2) a_2^1(k)] \ . \tag{33}$$

The observation should be made that C_S^1 and C_D^1 are real, but C_S^0 is purely imaginary owing to the fact that N_{d^*} is imaginary.

III. MODELS AND RESULTS

As mentioned in the Introduction, our aims are to investigate the dependence of the $^3H \rightarrow n+d$ vertex on P_D, the percentage D-state component in the deuteron wave function, and to investigate the sensitivity of the $^3H \rightarrow n+d^*$ asymptotic norm to the $^1S_0$ two-nucleon, low-energy scattering parameters. For the first case, we use models that allow P_D to vary while holding the following quantities fixed: $^1S_0$ interaction, deuteron binding energy, deuteron quadrupole moment, triplet scattering length, and triplet effective range. Such models for the two-nucleon $^3S_1$-$^3D_1$ interaction already exist from the work of Ioannides and Johnson (IJ),[10] Phillips (P),[11] and the present authors (GL).[12] P_D ranges in integer steps from 0% to 10% including a model with $P_D = 5.5\%$. For the $^3H \rightarrow n+d^*$ case, we hold the $^3S_1$-$^3D_1$ two-nucleon interaction fixed and vary the $^1S_0$ two-nucleon interaction by changing the low-energy parameters r_{0_s} and a_s. Models that vary r_{0_s} (a_s fixed) and a_s (r_{0_s} fixed) exist from earlier work of the present authors.[12]

The two-nucleon input and the corresponding calculated properties of ^3H are given in Table I. The ten IJ models, the three P models, model GL-OA, and model GL-4A serve as the fifteen models in which the $^1S_0$ interaction remains fixed. Various combinations of the P and GL models are used to investigate the situation where the $^1S_0$ interaction is changed. The calculated properties of ^3H given in the right-most five columns are obtained by solving Eqs. (A19)–(A21) in Appendix A and constructing the wave function components according to Eqs. (A2)–(A4). P_S^H, $P_{S'}^H$, P_D^H, and P_P^H represent the percentage S-state (symmetric), S-state (mixed symmetric), D-state, and P-state component in the ^3H wave function, respectively.

The structure of the ^3H wave function and the ^3H binding energy for the fifteen models where the $^1S_0$ NN interaction remains fixed ($a_s = -16.85$ fm and $r_{0_s} = 2.84$ fm) possess striking dependences on P_D. Most notable is the highly correlated ($r^2 = 0.998$, where r^2 is the correlation coefficient) *linear* dependence of P_S^H and P_D^H on P_D, where the slopes have equal magnitudes, but opposite signs

$$P_S^H = (-1.32 \pm 0.02) P_D + (98.5 \pm 0.1) \tag{34}$$

and

$$P_D^H = (1.31 \pm 0.02) P_D - (0.2 \pm 0.1) \ . \tag{35}$$

Though P_P^H is linearly correlated ($r^2 = 0.957$) with P_D,

TABLE I. Input and properties of ^{3}H models.

	Two-nucleon input					Calculated properties of ^{3}H				
Model	a_t (fm)	r_{0_t} (fm)	P_D (%)	a_s (fm)	r_{0_s} (fm)	B_3 (MeV)	P_S^H (%)	$P_{S'}^H$ (%)	P_D^H (%)	P_P^H (%)
IJ-1[a]	5.376	1.704	0.999	−16.85	2.84	9.973	97.55	1.71	0.74	0.5×10^{-3}
-2	5.389	1.705	1.999	−16.85	2.84	9.461	96.12	1.71	2.16	0.4×10^{-2}
-3	5.383	1.704	3.001	−16.85	2.84	9.018	94.61	1.73	3.65	0.01
-4	5.400	1.704	3.998	−16.85	2.84	8.575	93.16	1.74	5.08	0.02
-5	5.384	1.701	4.995	−16.85	2.84	8.238	91.73	1.75	6.49	0.03
-6	5.378	1.700	5.994	−16.85	2.84	7.923	90.38	1.75	7.83	0.04
-7	5.373	1.697	7.003	−16.85	2.84	7.635	89.08	1.74	9.12	0.06
-8	5.380	1.694	8.010	−16.85	2.84	7.352	87.87	1.73	10.33	0.06
-9	5.367	1.691	9.012	−16.85	2.84	7.126	86.69	1.72	11.52	0.07
-10	5.363	1.690	9.995	−16.85	2.84	6.905	85.59	1.70	12.63	0.08
P-4[b]	5.397	1.727	4.000	−16.85	2.84	8.568	93.18	1.70	5.10	0.02
-5.5	5.400	1.725	5.502	−16.85	2.84	8.032	91.09	1.71	7.16	0.04
-7	5.391	1.722	6.999	−16.85	2.84	7.598	89.14	1.70	9.10	0.06
GL-0A[c]	5.433	1.761	0	−16.85	2.84	10.14	98.32	1.68	0	0
-0B	5.433	1.761	0	−23.20	2.73	10.74	98.56	1.44	0	0
GL-4A[d]	5.378	1.698	4.159	−16.85	2.84	8.559	92.89	1.75	5.33	0.02
-4B	5.397	1.727	4.000	−20.36	2.85	8.711	93.24	1.66	5.08	0.02
-4C	5.397	1.727	4.000	−20.41	2.70	9.010	93.49	1.43	5.06	0.02
Experiment	5.425(4)	1.749(8)	(nn)	−17(1)	2.84(3)	8.482				
			(np)	−23.72(2)	2.73(3)					

[a]Triplet input, Ref. 10: $B_d=2.226$ MeV and $Q_d=0.2739$ fm^2. Singlet input, Ref. 12.
[b]Triplet input, Ref. 11: $B_d=2.225$ MeV and $Q_d=0.282\pm0.001$ fm^2. Singlet input, Ref. 12.
[c]Reference 12: $B_d=2.225$ MeV and $Q_d=0$. Note: $Q_d^{exp}=0.286$ fm^2.
[d]Reference 12, except for triplet in 4B and 4C which is P-4 from above.

TABLE II. Calculated $^3H \rightarrow n + d(d^*)$ vertex properties.

Model	μ (fm^{-1})	C_S^1	C_D^1	μ^* (fm^{-1})	C_S^0	D_0 (MeV fm$^{3/2}$)	D_2 (fm^2)	$\tilde{D}_2$ (fm^2)	$f_0(0)$ (fm$^{3/2}$)	$\pi\mu^{3/2}f_0(0)$
IJ-1	0.4991	1.884	0.263	0.562	$-0.935i$	177.7	−0.312	−0.560	1.456	1.613
-2	0.4824	1.878	0.139	0.548	$-0.952i$	173.4	−0.262	−0.318	1.522	1.602
-3	0.4674	1.861	0.109	0.534	$-0.963i$	170.0	−0.244	−0.268	1.589	1.595
-4	0.4519	1.840	0.0924	0.521	$-0.973i$	165.8	−0.234	−0.246	1.658	1.582
-5	0.4397	1.823	0.0822	0.510	$-0.982i$	163.1	−0.228	−0.233	1.722	1.577
-6	0.4280	1.806	0.0745	0.500	$-0.991i$	160.2	−0.224	−0.225	1.785	1.570
-7	0.4171	1.788	0.0685	0.491	$-0.999i$	157.4	−0.220	−0.220	1.847	1.563
-8	0.4060	1.770	0.0631	0.485	$-1.007i$	154.3	−0.220	−0.216	1.911	1.553
-9	0.3970	1.753	0.0591	0.477	$-1.014i$	152.1	−0.219	−0.214	1.970	1.548
-10	0.3879	1.736	0.0553	0.470	$-1.022i$	149.6	−0.217	−0.212	2.030	1.541
P-4	0.4516	1.844	0.0934	0.524	$-0.982i$	166.5	−0.236	−0.248	1.667	1.589
-5.5	0.4321	1.818	0.0786	0.504	$-0.994i$	161.5	−0.228	−0.232	1.766	1.576
-7	0.4156	1.791	0.0689	0.493	$-1.007i$	157.3	−0.224	−0.223	1.859	1.565
GL-0A	0.5053	1.921	0	0.567	$-0.959i$	179.5	0	0	1.440	1.625
-0B	0.5241	1.944	0	0.586	$-0.835i$	184.1	0	0	1.373	1.636
GL-4A	0.4513	1.837	0.0909	0.520	$-0.973i$	166.0	−0.232	−0.243	1.664	1.585
-4B	0.4567	1.864	0.0950	0.526	$-0.904i$	168.6	−0.233	−0.244	1.650	1.600
-4C	0.4671	1.860	0.0989	0.535	$-0.906i$	169.8	−0.230	−0.244	1.589	1.594
Experiment										
	0.4484	1.82 ±0.05[a]	?	?	?	163±2[b]	−0.279 ±0.012[a,c]			

[a]See Table I of Ref. 4.
[b]Reference 14.
[c]Reference 15.

$$P_P^H = (9.0\pm0.6)\times10^{-3}P_D - (1.1\pm0.3)\times10^{-2}\,, \quad (36)$$

its contribution to the overall normalization is negligible. Thus, since $P_{S'}^H$ is independent of P_D, its value being determined primarily by the difference between the S-wave singlet and triplet two-nucleon interactions,[13]

$$P_{S'}^H = 1.71\pm0.02\,, \quad (37)$$

TABLE III. Calculated $^3H \rightarrow n + d$ vertex properties.

Model	$-\pi\mu^{7/2}f_0(0)D_2$	P_{nd}^S	P_{nd}^D	$P_{nd}=P_{nd}^S+P_{nd}^D$
IJ-1	0.125	0.427	0.138×10^{-2}	0.428
-2	0.0977	0.428	0.307×10^{-2}	0.431
-3	0.0850	0.429	0.429×10^{-2}	0.433
-4	0.0756	0.431	0.512×10^{-2}	0.436
-5	0.0695	0.431	0.574×10^{-2}	0.437
-6	0.0644	0.432	0.618×10^{-2}	0.438
-7	0.0598	0.432	0.650×10^{-2}	0.438
-8	0.0563	0.433	0.669×10^{-2}	0.440
-9	0.0534	0.433	0.683×10^{-2}	0.440
-10	0.0503	0.433	0.689×10^{-2}	0.440
P-4	0.0765	0.431	0.514×10^{-2}	0.436
-5.5	0.0671	0.432	0.599×10^{-2}	0.438
-7	0.0605	0.432	0.650×10^{-2}	0.438
GL-0A	0	0.428	0	0.428
-0B	0	0.425	0	0.425
GL-4A	0.0748	0.430	0.525×10^{-2}	0.435
-4B	0.0778	0.430	0.511×10^{-2}	0.435
-4C	0.0780	0.428	0.513×10^{-2}	0.433

it is clear that P_S^H and P_D^H must be related as in Eqs. (34) and (35). Specifically, we have

$$P_S^H + P_{S'}^H + P_D^H = 100.0 \pm 0.2 \ . \tag{38}$$

The linear relationship between P_D^H (or P_S^H) and P_D is present in a summary of other exact three-body calculations by Friar.[7] Friar estimates the slope of his compilation to be 10/7, close to the present systematic analysis. Within the context of a nonrelativistic three-body theory, it would be enlightening to see the origin of this relationship uncovered. Perhaps bearing on a deeper understanding of the connection between P_D^H and P_D is comprehension of the decrease in the ^{3}H binding energy (B_3) as P_D increases. For the models under consideration, we get

$$B_3 = (-0.34 \pm 0.02) P_D + (10.09 \pm 0.08) \text{ MeV} \ , \tag{39}$$

where the correlation is $r^2 = 0.986$. As the role of the longer range tensor force grows (P_D increasing) the binding of the more compact ^{3}H (relative to ^{2}H) decreases.

The calculated results for the $^3\text{H} \to \text{n} + \text{d}$ asymptotic normalization constants, distorted-wave parameters, and fraction of neutron-deuteron component in the ^{3}H wave function are given in Tables II and III. Also tabulated in Tables II and III are "constant vertex" approximations to the asymptotic normalization constants: $\pi\mu^{3/2} f_0(0)$ for the S wave and $-\pi\mu^{7/2} f_0(0) D_2$ for the D wave. These approximations are derived by writing the momentum-distribution amplitudes for low-q values, $q^2 \lesssim \mu^2$, as

$$f_0(q) \cong \frac{\mu^2 f_0(0)}{q^2 + \mu^2} \tag{40}$$

and

$$f_2(q) \cong -\frac{\mu^2 q^2 f_0(0) D_2}{q^2 + \mu^2} \ ; \tag{41}$$

i.e., assuming constant vertex amplitudes.[16,8] It follows then, from Eq. (17), that the asymptotic norms are given in this approximation by

$$C_S^1 \sim \pi\mu^{3/2} f_0(0) \tag{42}$$

and

$$C_D^1 \sim -\pi\mu^{7/2} f_0(0) D_2 \ . \tag{43}$$

As is clear, the $f_l(q)$ are the key quantities in determining the $^3\text{H} \to \text{n} + \text{d}$ structure. Therefore, in Table IV, we tabulate the momentum distribution amplitudes for the IJ-4 and IJ-7 models in order that they be available for other applications.

The results for the $^3\text{H} \to \text{n} + \text{d}^*$ asymptotic normalization constant, C_S^0, are tabulated in the sixth column of Table II. These values must be calculated with care owing to the logarithmic singularity (branch cut) in the integrand of Eq. (33). As explained in Appendix B, this occurs because $K^2 < \mu^{*2}$. It can also occur for the $^3\text{H} \to \text{n} + \text{d}$ asymptotic norms whenever $B_3 \gtrsim 8.9$ MeV ($B_2 = 2.225$ MeV), since then $K^2 < \mu^2$.

IV. DISCUSSION

A. $^3\text{H} \to \text{n} + \text{d}$

1. *Asymptotic norms*

The dependence of the asymptotic norms on P_D is most striking. In Table II, considering the 15 models with the same $^1S_0$ NN interaction, we find that C_S^1 decreases linearly with P_D and that C_D^1 seems to be best fit employing a reciprocal dependence on P_D (see Figs. 2 and 3). Specifically, we find that

$$C_S^1 = (-1.77 \pm 0.04) \times 10^{-2} P_D + (1.913 \pm 0.003) \ , \tag{44}$$

TABLE IV. Momentum-distribution amplitudes (fm$^{3/2}$).

q (fm^{-1})	$P_D = 4\%$		$P_D = 7\%$	
	$f_0(q)$	$f_2(q)$	$f_0(q)$	$f_2(q)$
0	1.658	0	1.847	0
0.05	1.635	9.566×10^{-4}	1.818	1.008×10^{-3}
0.1	1.569	3.666×10^{-3}	1.733	3.846
0.2	1.346	1.250×10^{-2}	1.454	1.292×10^{-2}
0.3	1.077	2.227	1.132	2.267
0.4	8.274×10^{-1}	2.996	8.462×10^{-1}	3.020
0.5	6.225	3.458	6.219	3.476
0.7	3.464	3.594	3.330	3.662
0.9	1.939	3.128	1.807	3.290
1.0	1.459	2.808	1.340	3.013
1.2	8.378×10^{-2}	2.151	7.473×10^{-2}	2.414
1.4	4.892	1.573	4.225	1.852
1.6	2.901	1.117	2.411	1.379
1.8	1.745	7.778×10^{-3}	1.381	1.005
2.0	1.063	5.348	7.898×10^{-3}	7.213×10^{-3}
2.2	6.546×10^{-3}	3.651	4.471	5.121
2.4	4.072	2.481	2.476	3.606
2.6	2.554	1.683	1.315	2.524
2.8	1.614	1.141	6.439×10^{-4}	1.758
3.0	1.026	7.43×10^{-4}	2.626	1.222

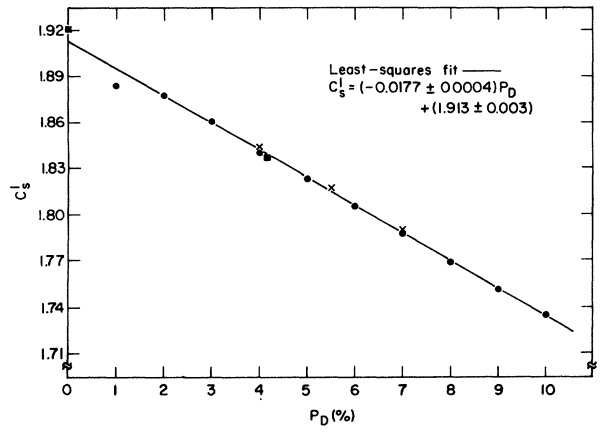

FIG. 2. C_S^1 as a function of P_D. Solid line is least-squares fit to IJ models (●), P models (×), GL-0A (✱), and GL-4A (■).

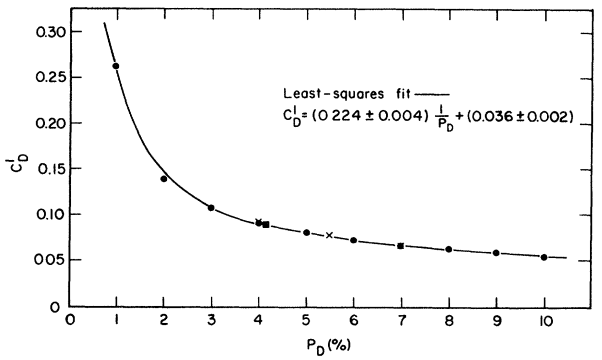

FIG. 3. C_D^1 as a function of P_D. Solid line is least-squares fit to IJ models (●), P model (×), and GL-4A (■).

with $r^2=0.994$, and

$$C_D^1=(2.24\pm0.04)\times10^{-1}\frac{1}{P_D}+(3.6\pm0.2)\times10^{-2}\ , \tag{45}$$

with $r^2=0.997$ (where model GL-0A has been dropped). Let us compare these results to those of the deuteron, d→n+p, given in Table V. For the deuteron, C_S^d is essentially a constant independent of P_D. This occurs because C_S^d is determined primarily by two parameters:[17] γ and r_{0_t}. Since these parameters are held fixed,

$$C_S^d \cong \frac{1}{(1-\gamma r_{0_t})^{1/2}} \tag{46}$$

remains unchanged. In contrast, the decrease in the neutron-deuteron binding as P_D increases, expressed through μ, means the exponential falloff of $u_0(\rho)$ is less rapid as P_D increases. Since P_{nd}^S is essentially independent of P_D (see Table III), i.e., all the $u_0(\rho)$ are normalized the same, C_S^1 decreases to compensate for the greater contribution to the normalization of the long-range part of $u_0(\rho)$. On the other hand, C_D^d of the deuteron, just like C_D^1, appears to best reflect a reciprocal dependence on P_D. The same 14 models used for Eq. (45) yield

$$C_D^d=(6.6\pm0.3)\times10^{-2}\frac{1}{P_D}+(2.2\pm0.1)\times10^{-2}\ . \tag{47}$$

Such behavior is certainly peculiar, since C_D^d and C_D^1 both vanish when $P_D=0$. Such behavior is indicative of forcing the $^3S_1$-$^3D_1$ interaction with $P_D<4\%$ to the constraints indicated in Table I—especially a *fixed* value of the quadrupole moment, Q_d. In the case of the triton, as mentioned in Appendix B, we get the abnormal relationship that $B_3>4B_2$ when $P_D<4\%$. Regardless, under such constraints, it is clear that C_D^1 *decreases gradually with* P_D for $P_D \geq 4\%$.

TABLE V. Calculated d→n + p vertex properties.

Model	C_S^d	C_D^d	$\eta=C_S^d/C_D^d$	D_2^d	$\tilde{D}_2^d$
IJ-1	1.283	0.0919	0.0716	−1.069	−1.335
-2	1.284	0.0495	0.0386	−0.6731	−0.7194
-3	1.284	0.0410	0.0319	−0.5766	−0.5950
-4	1.284	0.0371	0.0289	−0.5311	−0.5393
-5	1.285	0.0350	0.0272	−0.5049	−0.5078
-6	1.285	0.0336	0.0262	−0.4881	−0.4875
-7	1.286	0.0327	0.0254	−0.4772	−0.4742
-8	1.286	0.0320	0.0249	−0.4692	−0.4643
-9	1.286	0.0315	0.0245	−0.4633	−0.4568
-10	1.287	0.0311	0.0242	−0.4586	−0.4507
P-4	1.290	0.0375	0.0291	−0.5340	−0.5421
-5.5	1.291	0.0347	0.0268	−0.4999	−0.5006
-7	1.291	0.0331	0.0256	−0.4813	−0.4780
GL-0A	1.292	0	0	0	0
GL-4A	1.283	0.0366	0.0286	−0.5252	−0.5323
Experiment	1.299[a]		0.0272(4)[b]		

[a]Reference 17.
[b]Reference 18.

The variation of C_S^1 with P_D is slow enough that all the models with $3\% < P_D < 8\%$ (the standard range) are within experimental errors. Unfortunately, a direct experimental determination of C_D^1 has not yet been made. Nonetheless, values for C_S^1 and C_D^1 from a five-channel calculation using the Reid soft core potential ($^1S_0, ^3S_1$-$^3D_1$), hereafter denoted RSC5, are available.[4] The RSC5 values resemble the separable-model results that have $P_D \sim 7$–8%. The RSC potential gives $P_D = 6.47\%$ and leads to a smaller ^{3}H binding energy ($B_3 = 7.022$ MeV) than the separable models with comparable P_D. The latter attribute accounts, qualitatively, for the somewhat lower values of C_S^1 and C_D^1 for the RSC5 compared to a separable model with the same P_D.

It is tempting to assume a constant $^3\mathrm{H} \to \mathrm{n}+\mathrm{d}$ vertex amplitude in order to simplify calculations containing this vertex.[16] When such an assumption is made, the momentum distribution amplitudes are given by Eqs. (40) and (41), while the asymptotic norms are given by Eqs. (42) and (43). When the asymptotic norms are evaluated in this approximation, last column of Table II and first column of Table III, the asymptotic norms are *underestimated* by 10–20%. This is a clear indication that the $^3\mathrm{H} \to \mathrm{n}+\mathrm{d}$ vertex-amplitude momentum dependence is important, even at small values of q, $q^2 \lesssim \mu^2$. Such a constant-vertex approximation for the deuteron, $\mathrm{d} \to \mathrm{n}+\mathrm{p}$, leads to only a 3% (2%) underestimate of C_S^{d} (C_D^{d}). The reason the approximation works so well for the deuteron is due to the size of the inverse-range parameters in the S- and D-wave vertex amplitudes. The momentum dependence of the deuteron vertex amplitudes is given by the $g_l^1(q)$ with the inverse-range parameters, β_l^1. Neglecting the q dependence of the $g_l^1(q)$ is justified for $q^2 \ll (\beta_l^1)^2$ *and* is valid at the deuteron pole, $q = i\gamma$, since $\gamma^2 \ll (\beta_l^1)^2$ [$\gamma^2 = 0.054$ fm^{-2}, $(\beta_0^1)^2 = 1.782$ fm^{-2}, and $(\beta_2^1)^2 = 2.362$ fm^{-2} for IJ-4)]. Evidently, the "equivalent" inverse-range parameter and μ are more comparable in size for the $^3\mathrm{H} \to \mathrm{n}+\mathrm{d}$ vertex.

Finally, we note that C_S^1 is insensitive ($< 2\%$ variation) to changes in the $^1S_0$ NN parameters, whereas C_D^1 is mildly sensitive ($\lesssim 5\%$ variation) to changes in the $^1S_0$ interaction.

2. *Distorted-wave parameters*

The present work on the DW parameters D_0 and D_2 complements the results of Ioannides *et al.* (INS) (Ref. 9) and Borberly and Doleschall (BD).[14] Our effort adds a systematic investigation of the dependence of these parameters upon P_D and examines the validity of approximating D_2 by $\tilde{D}_2$, Eq. (23).

By least-squares fitting the results for D_0 given in Table II (models with the same $^1S_0$ interaction), it is clear that D_0 decreases linearly with P_D:

$$D_0 = (-3.09 \pm 0.08) P_D + (179.2 \pm 0.5) \text{ MeV fm}^{3/2} , \tag{48}$$

and $r^2 = 0.993$. INS find that D_0 decreases when P_D is increased, but their phenomenological ^{3}H ground-state wave function does not permit them to make an accurate estimate of the decrease. BD calculate a decrease in D_0 of 7.9 MeV fm$^{3/2}$ in going from $P_D = 4\%$ to $P_D = 7\%$ (see their models $2^1S_0R, 1T4RA$ and $2^1S_0R, 1T7RA$). This magnitude of decrease is roughly consistent with our prediction ($\Delta P_D = 3$):

$$\Delta D_0 = (-3.09 \pm 0.08) \Delta P_D = -9.3 \pm 0.3 \text{ MeV fm}^{3/2} . \tag{49}$$

The origin of the decrease is the decrease in $(B_3 - B_2)$ (equivalently μ) as P_D increases, because $f(0)$ actually increases with P_D [see below and Eq. (20)]. Note that to have values of D_0 within the experimental range, P_D must lie between 4% and 6%.

Similar to C_D^1, if we exclude the values for $P_D < 4\%$, we find that D_2 decreases almost linearly with P_D. A least-squares fit to those 11 models with the same $^1S_0$ NN interaction and $P_D \geq 4\%$ yields

$$D_2 = (3.0 \pm 0.4) \times 10^{-3} P_D - (0.244 \pm 0.002) \text{ fm}^2 , \tag{50}$$

with $r^2 = 0.894$. Allowing for the limitations of extracting D_2 from experiment,[4,15] one can conclude that the values of D_2 for $P_D \geq 4\%$ lie just slightly below the current experimental value. BD suggest a "best" value based on their calculations of -0.225 ± 0.005 fm^2. This encompasses our results for $5\% \lesssim P_D \lesssim 8\%$.

How closely does $\tilde{D}_2$ approximate D_2? As can be seen in Fig. 4, for values of P_D between 4% and 7%, the error is $\lesssim 5\%$ and $\lesssim 2\%$ between $P_D = 5\%$ and 7%, respectively. Clearly, for the deuteron (Table V) the approximation is even better over the same range. $\tilde{D}_2$ has been calculated[4] for the RSC5 model with the result of 0.243 fm^2, larger than the separable results with comparable P_D. This occurs because of the smaller μ^2 (due to the smaller B_3) in the RSC5 result, since the ratio C_D^1/C_S^1 is actually somewhat smaller than for the separable models. Finally, we note that D_0 and D_2 are not sensitive to the $^1S_0$ NN parameters.

3. *Fraction of nucleon-deuteron component*

The fraction of S-wave neutron-deuteron component in the ^{3}H wave function is independent of P_D (see Table III). Not only is it independent of P_D, it is not sensitive to the $^1S_0$ NN low-energy parameters. Neither is the fraction of D-wave nucleon-deuteron component sensitive to the $^1S_0$ NN interaction, but it is sensitive to the value of P_D. P_{nd}^D rises fairly rapidly from zero to an asymptote of $\sim 0.7 \times 10^{-2}$ for $0 \leq P_D \lesssim 10\%$. The models suggest that

$$P_{\mathrm{nd}}^S = 0.430 \pm 0.002 , \tag{51a}$$

independent of P_D, and that

$$P_{\mathrm{nd}}^D \sim 0.6 \times 10^{-2} \tag{51b}$$

for $4\% \lesssim P_D \lesssim 7\%$.

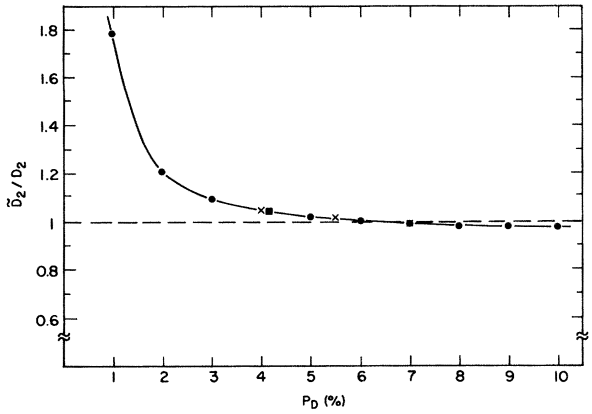

FIG. 4. Ratio of $\tilde{D}_2$ to D_2. The solid line is only to guide the eye through the calculated values of the ratio for the IJ models (●), P models (×), and GL-4A (■).

4. *Momentum-distribution amplitudes*

The momentum-distribution amplitudes, $f_l(q)$, are plotted in Fig. 5 for $P_D=0\%$, 4%, and 7% (see Table IV). As P_D increases, $f_0(0)$ rises linearly (see Fig. 6) and $f_0(q)$ for $q \gtrsim 1$ fm^{-1} decreases (remember that P_{nd}^S is independent of P_D). The loss of higher momentum contributions in $f_0(q)$ as P_D increases is made up by the increasing contribution of $f_2(q)$. Moreover, it can clearly be seen in Fig. 7, by means of a Chew-Low plot,[19] that the assumption of a constant $^3H \rightarrow n + d$ vertex amplitude (S wave) is not justified even for a limited range of q. The dashed line represents the constant vertex approximation, whereas the momentum dependence of the vertex draws $1/f_0(q)$ away from the dashed line almost immediately beyond $q=0$. Similar conclusions can be reached with a D-wave Chew-Low plot. This makes it even more clear that the approximations for the asymptotic norms given in Eqs. (42) and (43) are incorrect.

The $^3H \rightarrow n + d$ momentum distributions for IJ-4 and IJ-7 are plotted in Fig. 8 against the data extracted from the recent ^{3}He(e,e'p) experiment at Saclay.[3] The absolute uncertainty involved in such an extraction is on the order of 10—15% due to the assumption of pole dominance and the ambiguity associated with the "off-shell" electron-proton cross section [see Eq. (6)]. Therefore, within this framework, we can say the models are consistent with experiment for $q \lesssim 100$ MeV/$c \sim \mu$, the expected range of validity of pole dominance.[16,8] At higher momentum tranfers, the theories exceed experiment. Such behavior is also found in more sophisticated models like the RSC.[3] This emphasizes that the pole-dominance assumption at the higher-momentum transfers is invalid.

B. $^3H \rightarrow n + d^*$

1. *Asymptotic norm*

C_S^0 is correlated linearly with P_D. For the 15 models with the same $^1S_0$ NN interaction, we find

$$C_S^0 = -i[(8.2\pm0.8)\times10^{-3}P_D + (0.942\pm0.005)] \quad (52)$$

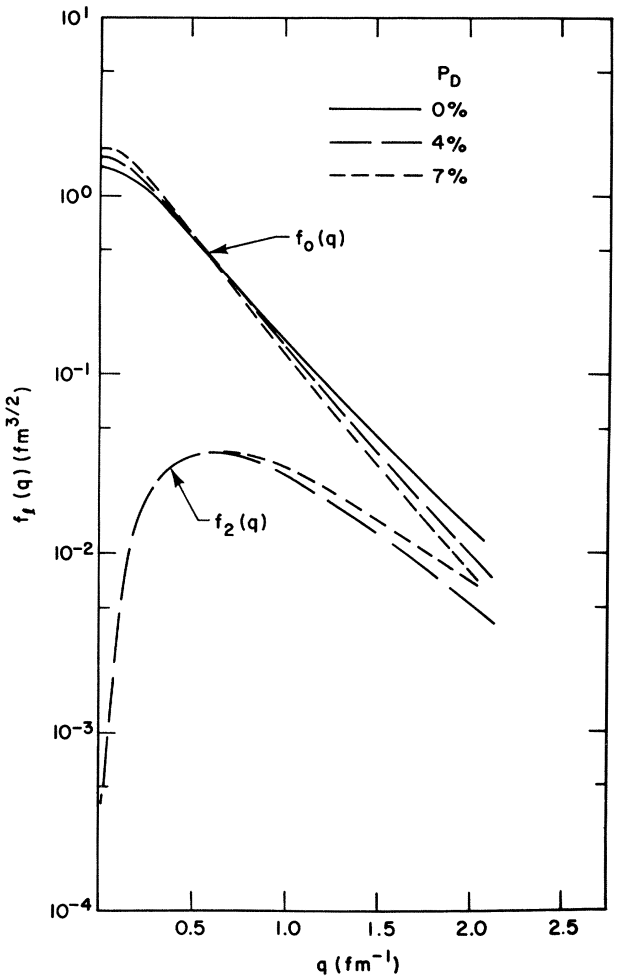

FIG. 5. Momentum-distribution amplitudes for selected IJ models.

with $r^2=0.91$. Similarly as with C_S^1, this is a binding effect though it cannot be reasoned through as we did for C_S^1, since C_S^0 is the coefficient of a non-normalizable function (ϕ_{d^*} is not normalizable). What is even more striking is the sensitivity of C_S^0 to the low-energy properties of the

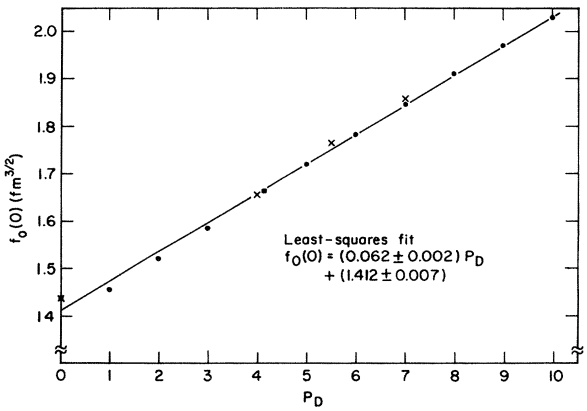

FIG. 6. $f_0(0)$ as a function of P_D. Solid line is least-squares fit to IJ models (●), P models (×), GL-0A (✱), and GL-4A (■).

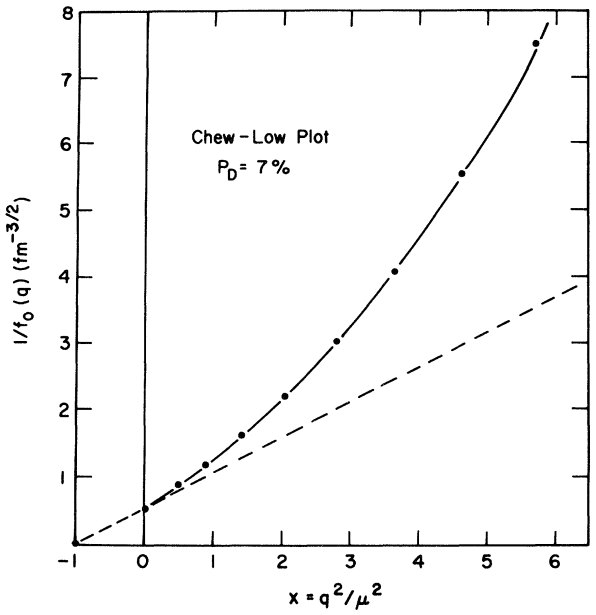

FIG. 7. Chew-Low plot for the $^3H \rightarrow n + d$ vertex. The dashed line represents a constant vertex normalized to the IJ-7 model and the solid line illustrates the momentum dependence of the $^3H \rightarrow n + d$ vertex for the IJ-7 model.

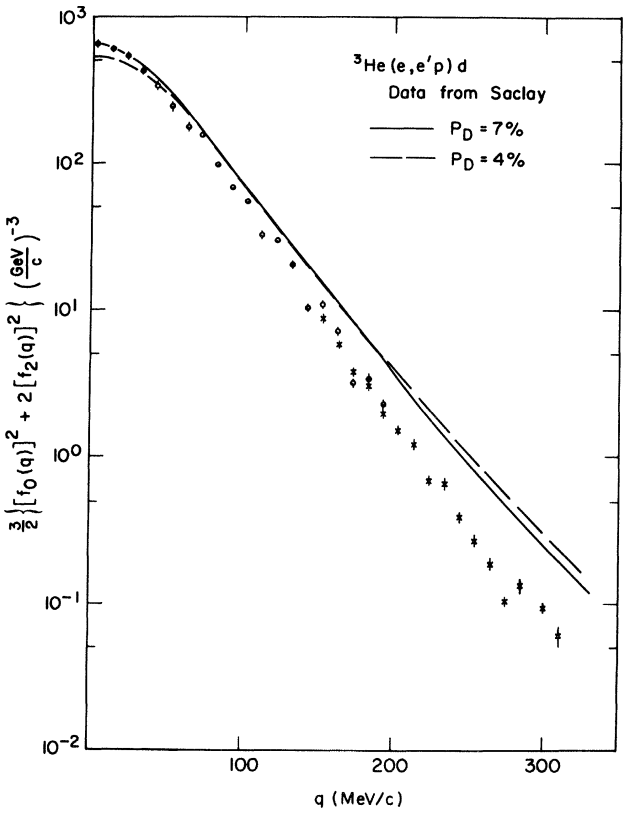

FIG. 8. $^3H \rightarrow n + d$ momentum distribution for the IJ-4 (— — —) and IJ-7 (——) models. The data points are from Ref. 3.

$^1S_0$ interaction. Changing r_{0_s} from 2.85 to 2.70 fm leads to almost no change in C_S^0 even though B_3 changes from 8.711 to 9.010 MeV. On the other hand, decreasing a_s from -16.85 to -20.36 or from -16.85 to -23.20 leads to a change in C_S^0 of $\sim 0.1i$. Changing a_s in this way decreases γ_0, while changing r_{0_s} from 2.85 to 2.70 fm hardly changes γ_0. Now, $C_S^0 \sim N_0 \sim \gamma_0^{1/2}$, and the change in γ_0 can account for the change in C_S^0 since μ^* does not shift by a large amount. Clearly, assuming charge independence in dealing with this parameter is an $\sim 10\%$ approximation.

One local-potential calculation of C_S^0 exists where the NN interaction is a one-boson-exchange (OBE) model ($a_s = -23.83$ fm and $r_{0_s} = 2.703$ fm).[5] This model has a ^3H binding energy of 7.38 MeV and yields $C_S^0 = -0.831i$. This same model gives $C_S^1 = 1.61$. Compared to our models with $P_D = 4\%$ to 5%, typical of OBE models, these values are smaller in magnitude.

V. SUMMARY OF CONCLUSIONS

With a set of ^3H wave functions derived from separable NN interactions acting in the $^1S_0$ and $^3S_1$-$^3D_1$ partial waves, a systematic analysis of the $^3H \rightarrow n + d(d^*)$ vertices was made. The dependence of the $^3H \rightarrow n + d$ asymptotic normalization constants, the $^3H \rightarrow n + d$ distorted-wave parameters, the fractional n-d component in the ^3H wave function, and the $^3H \rightarrow n + d$ momentum distribution on the percentage D-wave component (P_D) in the deuteron was investigated. The sensitivity of the $^3H \rightarrow n + d^*$ asymptotic normalization constant to the low-energy parameters of the $^1S_0$ interaction was examined.

The *major* conclusions of this work can be summarized as follows (the reader is referred to Secs. III and IV for amplification of the models and details of the conclusions, respectively):

(1) The S-wave $^3H \rightarrow n + d$ asymptotic norm decreases *linearly* with P_D [Eq. (44)], while the D-wave asymptotic norm decreases *inversely* with P_D [Eq. (45)].

(2) The S-wave $^3H \rightarrow n + d$ distorted-wave parameter, D_0, decreases *linearly* with P_D [Eq. (48)] due to the decrease in n-d binding (to form ^3H) as P_D increases; the D-wave parameter, D_2, can be said to decrease almost linearly with P_D for $P_D \geq 4\%$ [Eq. (50)]. Approximation of D_2 using the asymptotic forms of the effective n-d S- and D-wave functions [Eq. (23)] leads to an overestimate of D_2 by $\sim 5\%$ for $P_D = 4\%$, which falls to an underestimate of $\sim 1\%$ for $P_D = 7\%$.

(3) The S-wave $^3H \rightarrow n + d$ asymptotic norm and the distorted-wave parameters, D_0 and D_2, are insensitive to changes in the low-energy parameters of the $^1S_0$ NN interaction, whereas the D-wave asymptotic norm is slightly sensitive to such changes (see Tables I and II).

(4) $^3H \rightarrow n + d$ asymptotic norms and distorted wave parameters calculated for the models, where the $^3S_1$-$^3D_1$ interaction generates P_D in the canonical band $4\% \lesssim P_D \lesssim 7\%$, are within present experimental limits. Moreover, models with low-energy parameters close to the Reid soft core NN potential yield results similar to a RSC five-channel calculation.

(5) The fraction of the n-d component in the ^3H models is 0.435 ± 0.004, to a good approximation independent of P_D (see Table III).

(6) Neglecting the momentum dependence of the $^3H \rightarrow n + d$ vertex amplitude leads to a $> 10\%$ error in the calculated asymptotic norms [See Eqs. (42) and (43) plus Tables II and III]. Furthermore, it is clear from a Chew-Low plot that a constant $^3H \rightarrow n + d$ vertex amplitude is a poor approximation (see Fig. 7).

(7) The $^3H \rightarrow n + d$ momentum distribution for the $P_D = 4\%$ or 7% models is in reasonable agreement with that extracted from the recent $^3He(e,e'p)d$ experiment at Saclay in the range of momentum transfer at the $^3H \rightarrow n + d$ vertex $0 \leq q \leq 0.5$ fm^{-1}, but is larger than the data for $q > 0.5$ fm^{-1} (see Fig. 8). Local-potential models show similar behavior relative to the data.[3]

(8) The $^3H \rightarrow n + d^*$ asymptotic norm is sensitive to changes in the NN singlet scattering length and it exhibits a slight dependence on P_D. The only existing local potential (OBE) calculation gives a result $\sim 6\%$ smaller in magnitude than the separable models with comparable P_D and equivalent low-energy $^1S_0$ NN interaction parameters.

The work of B.F.G. was performed under the auspices of the U.S. Department of Energy, while the work of D.R.L. was supported in part by the U. S. Department of Energy.

APPENDIX A

The purpose of this appendix is to give the explicit form of the ^3H wave function and related equations that were used to derive and calculate the results given in the main text. ^3H has total-angular-momentum, parity, and isospin quantum numbers $J^\pi I = \frac{1}{2}^+ \frac{1}{2}$. When the two-nucleon separable interactions are present in the $^1S_0$ and $^3S_1$-$^3D_1$ waves, the ^3H wave function has the form

$$\Psi^{[1/2]} = \frac{N}{2}[\Psi_0^{[1/2]}(\hat{123}) + \Psi_1^{[1/2]}(\hat{123}) + \Psi_2^{[1/2]}(\hat{123})] , \tag{A1}$$

where

$$\Psi_0^{[1/2]} = [\Psi^{[0]S} \times \xi^{[1/2]a}]^{[1/2]} + [\Psi^{[0]'} \times \xi^{[1/2]''}]^{[1/2]} - [\Psi^{[0]''} \times \xi^{[1/2]'}]^{[1/2]} , \tag{A2}$$

$$\Psi_1^{[1/2]} = [\Psi^{[1]S} \times \xi^{[1/2]a}]^{[1/2]} + [\psi^{[1]'} \times \xi^{[1/2]''}]^{[1/2]} - [\Psi^{[1]''} \times \xi^{[1/2]'}]^{[1/2]} - [\Psi^{[1]'} \times \chi^{[3/2]S}]^{[1/2]}\eta'' + [\Psi^{[1]''} \times \chi^{[3/2]S}]^{[1/2]}\eta' , \tag{A3}$$

and

$$\Psi_2^{[1/2]} = [\Psi^{[2]'} \times \chi^{[3/2]S}]^{[1/2]}\eta'' - [\Psi^{[2]''} \times \chi^{[3/2]S}]^{[1/2]}\eta' . \tag{A4}$$

The spin-$\frac{1}{2}$ (χ), isospin-$\frac{1}{2}$ (η) functions have the form

$$\xi^a = \frac{1}{\sqrt{2}}(\chi'\eta'' - \chi''\eta') , \tag{A5}$$

$$\xi' = \frac{1}{\sqrt{2}}(\chi'\eta'' + \chi''\eta') , \tag{A6}$$

and

$$\xi'' = \frac{1}{\sqrt{2}}(\chi'\eta' - \chi''\eta'') , \tag{A7}$$

where $(a,','')$ mean antisymmetric under exchange of any nucleon pair, antisymmetric under exchange of the (23) pair, and symmetric under exchange of the (23) pair, respectively. This notation applies elsewhere in the above equations with the addition that "S" means symmetric under exchange of any nucleon pair. The spatial functions have the form

$$\Psi^S(\overline{123}) = g(1,\overline{23}) + g(2,\overline{31}) + g(3,\overline{12}) , \tag{A8}$$

$$\Psi'(\hat{123}) = \frac{\sqrt{3}}{2}[h(3,\overline{12}) - h(2,\overline{31})] , \tag{A9}$$

and

$$\Psi''(1\overline{23}) = -h(1,\overline{23}) + \tfrac{1}{2}[h(2,\overline{31}) + h(3,\overline{12})] , \tag{A10}$$

where $(\hat{},^-)$ over particle numbers means antisymmetric or symmetric, respectively. In terms of the standard Yamaguchi[20] separable potential form factors and the three-body spectator functions, the spatial functions are given explicitly as

$$g^{[0]} = u^0 - v^1 , \tag{A11}$$

$$h^{[0]} = u^0 + v^1 , \tag{A12}$$

$$u^0 = a_0^0(1)g_0^0(23) , \tag{A13}$$

$$v^1 = a_0^1(1)g_0^1(23) - \tfrac{1}{2}a_2^1(1)g_2^1(23)4\pi[Y^{[2]}(1) \times Y^{[2]}(23)]^{[0]} , \tag{A14}$$

$$g^{[1]} = -\frac{\hat{1}}{\hat{\frac{1}{2}}\hat{2}}a_2^1(1)g_2^1(23)4\pi[Y^{[2]}(1) \times Y^{[2]}(23)]^{[1]} , \tag{A15}$$

$$h^{[1]} = -g^{[1]} , \tag{A16}$$

$$g^{[2]} \equiv 0 , \tag{A17}$$

and

$$h^{[2]}=-\tfrac{\hat{1}}{2}a_0^1(1)g_2^1(23)\sqrt{4\pi}Y^{[2]}(23)+\tfrac{\hat{1}}{2}a_2^1(1)g_0^1(23)\sqrt{4\pi}Y^{[2]}(1)+\frac{\hat{3}}{\frac{\hat{1}}{2}\hat{2}}a_2^1(1)g_2^1(23)4\pi[Y^{[2]}(1)\times Y^{[2]}(23)]^{[2]}\,, \quad \text{(A18)}$$

where $\hat{j}=(2j+1)^{1/2}$ and contrastandard spherical harmonics are related to the ordinary spherical harmonics by $Y_m^{[l]}(\hat{r})=(-i)^l Y_{lm}(\hat{r})$. In all the $g^{[l]}$ and $h^{[l]}$, the energy denominator, $(k_{23}^2+\frac{3}{4}p_1^2+K^2)^{-1}$, has been suppressed ($K^2=MB_3$, where B_3 is the three-nucleon binding energy). Finally, the N in Eq. (A1) is the normalization constant.

The spectator functions, a_l^S, are obtained by solving a coupled set of homogeneous integral equations. These equations are

$$D^0(p,K^2)a_0^0(p)=\pi\lambda_0\int_0^\infty k^2dk[{}_0^0I_0^0(p,k;K^2)a_0^0(k)-3_0^0I_0^1(p,k;K^2)a_0^1(k)+3_0^0I_2^1(p,k;K^2)a_2^1(k)]\,, \quad \text{(A19)}$$

$$D^1a_0^1=\pi\lambda_1\int_0^\infty k^2dk(-3_0^1I_0^0a_0^0+{}_0^1I_0^1a_0^1-{}_0^1I_2^1a_2^1)\,, \quad \text{(A20)}$$

and

$$D^1a_2^1=\pi\lambda_1\int_0^\infty k^2dk(3_2^1I_0^0a_0^0-{}_2^1I_0^1a_0^1+{}_2^1I_2^1a_2^1)\,, \quad \text{(A21)}$$

where

$$D^S(p,K^2)=1-\lambda_S\Lambda^S(p,K^2)\,, \quad \text{(A22)}$$

$$\Lambda^0=\int d^3k\frac{[g_0^0(k)]^2}{k^2+\frac{3}{4}p^2+K^2}\,, \quad \text{(A23)}$$

$$\Lambda^1=\int d^3k\frac{\sum_{l=0,2}[g_l^1(k)]^2}{k^2+\frac{3}{4}p^2+K^2}\,, \quad \text{(A24)}$$

$${}_0^0I_l^S=\int_{-1}^1dx\,\Delta^{-1}(k,p,x;K^2)g_0^0(q)g_l^S(q')P_l(\hat{k}\cdot\hat{q}')\,, \quad \text{(A25)}$$

$${}_0^1I_0^0=\int_{-1}^1dx\,\Delta^{-1}g_0^1(q)g_0^0(q')\,, \quad \text{(A26)}$$

$${}_0^1I_0^1=\int_{-1}^1dx\,\Delta^{-1}[g_0^1(q)g_0^1(q')-2g_2^1(q)g_2^1(q')P_2(\hat{q}\cdot\hat{q}')]\,, \quad \text{(A27)}$$

$${}_0^1I_2^1=\int_{-1}^1dx\,\Delta^{-1}\left\{g_0^1(q)g_2^1(q')P_2(\hat{k}\cdot\hat{q}')-2g_2^1(q)g_0^1(q')P_2(\hat{k}\cdot\hat{q})\right.$$
$$\left.+\frac{1}{\sqrt{2}}g_2^1(q)g_2^1(q')[1-P_2(\hat{k}\cdot\hat{q}')-P_2(\hat{k}\cdot\hat{q})-P_2(\hat{q}\cdot\hat{q}')]\right\}\,, \quad \text{(A28)}$$

$${}_2^1I_0^0=\int_{-1}^1dx\,\Delta^{-1}g_2^1(q)g_0^0(q')P_2(\hat{p}\cdot\hat{q})\,, \quad \text{(A29)}$$

$${}_2^1I_0^1=\int_{-1}^1dx\,\Delta^{-1}\left\{g_2^1(q)g_0^1(q')P_2(\hat{p}\cdot\hat{q})-2g_0^1(q)g_2^1(q')P_2(\hat{p}\cdot\hat{q}')\right.$$
$$\left.+\frac{1}{\sqrt{2}}g_2^1(q)g_2^1(q')[1-P_2(\hat{p}\cdot\hat{q})-P_2(\hat{p}\cdot\hat{q}')-P_2(\hat{q}\cdot\hat{q}')]\right\}\,, \quad \text{(A30)}$$

$${}_2^1I_2^1=\int_{-1}^1dx\,\Delta^{-1}\left\{-2g_0^1(q)g_0^1(q')P_2(\hat{p}\cdot\hat{k})+\frac{1}{\sqrt{2}}g_0^1(q)g_2^1(q')[1-P_2(\hat{k}\cdot\hat{q}')-P_2(\hat{p}\cdot\hat{k})-P_2(\hat{p}\cdot\hat{q}')]\right.$$
$$+\frac{1}{\sqrt{2}}g_2^1(q)g_0^1(q')[1-P_2(\hat{k}\cdot\hat{q})-P_2(\hat{p}\cdot\hat{k})-P_2(\hat{p}\cdot\hat{q})]$$
$$\left.+\tfrac{1}{4}g_2^1(q)g_2^1(q')[2P_2(\hat{k}\cdot\hat{q}')+2P_2(\hat{p}\cdot\hat{q})-P_2(\hat{k}\cdot\hat{q})-P_2(\hat{p}\cdot\hat{k})-P_2(\hat{q}\cdot\hat{q}')-P_2(\hat{p}\cdot\hat{q}')]\right\}\,, \quad \text{(A31)}$$

$$\Delta(k,p,x;K^2)=k^2+p^2+kpx+K^2\,, \quad \text{(A32)}$$

$$x=\hat{k}\cdot\hat{p}\,, \quad \text{(A33)}$$

$$\vec{q}=\vec{k}+\tfrac{1}{2}\vec{p}\,, \quad \text{(A34)}$$

$$\vec{q}\,'=\vec{p}+\tfrac{1}{2}\vec{k}\,, \quad \text{(A35)}$$

and $P_2(x)$ is a Legendre polynomial. The strength parameters of the interaction are the λ_S and the inverse ranges, β_l^S, define the interaction form factors

$$g_0^S(k)=[k^2+(\beta_0^S)^2]^{-1} \tag{A36}$$

and

$$g_2^1(k)=tk^2[k^2+(\beta_2^1)^2]^{-2}\ , \tag{A37}$$

where t controls the contribution of the D wave in the $^3S_1$-$^3D_1$ interaction.

APPENDIX B

In calculating the asymptotic normalization constants, integrals of the general form

$$\int_0^\infty k^2 dk\, I(p,k;K^2)a(k)\ , \tag{B1}$$

with $p=i\mu$ or $i\mu^*$ and

$$I(p,k;K^2)=\int_{-1}^{1} dx \frac{h(p,k;x)}{K^2+p^2+k^2+pkx}\ , \tag{B2}$$

are encountered. When $p=i\mu$, Eq. (B2) becomes

$$I(i\mu,k;K^2)=\frac{1}{i\mu k}\int_{-1}^{1} dx \frac{h(i\mu,k;x)}{x+\dfrac{k^2-k_0^2}{i\mu k}}\ , \tag{B3}$$

where $k_0^2=\mu^2-K^2=(K^2-4\gamma^2)/3$. For the models in Table II with $P_D<4\%$, $K^2>4\gamma^2$, or $k_0^2>0$. Likewise, when $p=i\mu^*$,

$$k_0^2=\mu^{*2}-K^2=(K^2-4\gamma^{*2})/3>0$$

for *all* the models. Under the condition $k_0^2>0$, $I(i\mu,k;K^2)$ [or $I(i\mu^*,k;K^2)$] possesses a cut singularity in the complex k plane along the curve defined by the equation

$$k=\tfrac{1}{2}\{-i\mu x+[\mu^2(1-x^2)-4\gamma^2]^{1/2}\}\ , \tag{B4}$$

that crosses the real k axis in the path of integration at k_0; i.e., $x=0$ and

$$k=\tfrac{1}{2}(\mu^2-4\gamma^2)^{1/2}=\left[K^2-\frac{4\gamma^2}{3}\right]^{1/2}=k_0\ . \tag{B5}$$

In numerically integrating over k in Eq. (B1), this logarithmic singularity must be considered.

In the present work, we used a subtraction to permit analytic expression of the logarithm:

$$\int_0^\infty dk\, I(i\mu,k;K^2)k^2a(k)=\int_0^\infty dk\int_{-1}^{1} dx \frac{h(i\mu,k;x)k^2a(k)-\phi(k)h(i\mu,k_0,0)k_0^2a(k_0)}{k_0^2-k^2+i\mu kx}$$

$$+h(i\mu,k_0;0)k_0^2a(k_0)\int_0^\infty dk\,\phi(k)\int_{-1}^{1} dx \frac{1}{k^2-k_0^2+ik\mu x}\ , \tag{B6}$$

where $\phi(k_0)=1$. The integrand of the first k integral on the right-hand side of Eq. (B6) has no logarithmic singularity. Therefore, since $x\neq 0$ on a Gaussian grid, the first integral is evaluated by standard numerical quadrature. The second k integral is handled as follows:

$$\int_0^\infty dk\,\phi(k)\int_{-1}^{1} dx \frac{1}{k^2-k_0^2+i\mu kx}=\int_0^\infty dk\,\phi(k)\frac{1}{ik\mu}\ln\frac{k^2-k_0^2+ik\mu}{k^2-k_0^2-ik\mu}\equiv\mathscr{S}\ , \tag{B7}$$

where a cut is crossed at $k=k_0$. Explicitly, we have

$$\mathscr{S}\equiv\int_0^{k_0} dk\,\phi(k)\frac{1}{ik\mu}\left[2\pi i+\ln\frac{k^2-k_0^2+ik\mu}{k^2-k_0^2-ik\mu}\right]+\int_{k_0}^\infty dk\,\phi(k)\frac{1}{ik\mu}\ln\frac{k^2-k_0^2+ik\mu}{k^2-k_0^2-ik\mu} \tag{B8}$$

$$=\frac{2\pi}{\mu}\int_0^{k_0}\frac{dk}{k}\phi(k)+\frac{1}{i\mu}\int_0^\infty\frac{dx}{k}\phi(k)\ln\frac{k^2-k_0^2+ik\mu}{k^2-k_0^2-ik\mu}\ . \tag{B9}$$

One might search for a $\phi(k)$ that would permit analytic evaluation of the integrals in Eq. (B9); nevertheless, we chose

$$\phi(k)=\frac{k^2a(k)}{k_0^2a(k_0)}\ , \tag{B10}$$

and carried out the integrations numerically.

[1]J. S. McCarthy, I. Sick, and R. R. Whitney, Phys. Rev. C 15, 1396 (1977); R. G. Arnold, B. T. Chertok, S. Rock, W. P. Schütz, Z. M. Szalata, D. Day, J. S. McCarthy, F. Martin, B. A. Mecking, I. Sick, and G. Tamas, Phys. Rev. Lett. 40, 1429 (1978).

[2]J. M. Cavedon, B. Frois, D. Goutte, M. Huet, Ph. Leconte, J. Martino, X.-H. Phan, S. K. Platchkov, S. E. Williamson, W. Boeglin, I. Sick, P. de Witt-Huberts, L. S. Cardman, and C. N. Papanicolas, Phys. Rev. Lett. 49, 986 (1982).

[3]E. Jans, P. Barreau, M. Bernheim, J. M. Finn, J. Morgenstern, J. Mougey, D. Tarnowski, S. Turck-Chieze, S. Frullani, F. Garibaldi, G. P. Capitani, E. de Sanctis, M. K. Brussel, and I. Sick, Phys. Rev. Lett. 49, 974 (1982).

[4]J. L. Friar, B. F. Gibson, D. R. Lehman, and G. L. Payne, Phys. Rev. C 25, 1616 (1982).

[5]E. P. Harper, D. R. Lehman, and F. Prats, Rev. Lett. 44, 237 (1980).

[6]R. V. Reid, Ann. Phys. (N.Y.) 50, 411 (1968).

[7]J. L. Friar, Phys. Rev. C 20, 325 (1979).

[8]D. R. Lehman, Phys. Rev. C 3, 1827 (1971); 6, 2023 (1972).

[9]A. A. Ioannides, M. A. Nagaragan, and R. Shyam, Nucl. Phys. A363, 150 (1981).

[10]A. A. Ioannides and R. C. Johnson, Phys. Rev. C 17, 1331 (1978).

[11]A. C. Phillips, Nucl. Phys. A107, 209 (1968).

[12]B. F. Gibson and D. R. Lehman, Phys. Rev. C 11, 29 (1975); see also, B. F. Gibson and G. J. Stephenson, Jr., *ibid.* 11, 1448 (1975); 8, 1222 (1973).

[13]D. R. Lehman, F. Prats, and B. F. Gibson, Phys. Rev. C 19, 310 (1979).

[14]I. Borbély and P. Doleschall, Phys. Lett. 113B, 443 (1982).

[15]S. Sen and L. D. Knutson, Phys. Rev. C 26, 257 (1982).

[16]I. S. Shapiro, in *Selected Topics in Nuclear Theory,* edited by F. Janouch (IAEA, Vienna, 1963), p. 85.

[17]T. E. O. Ericson and M. Rosa Clot, CERN report TH.3462, 1982.

[18]I. Borbély, W. Grüebler, V. König, P. A. Schmelzbach, and B. Jenny, Phys. Lett. 109B, 262 (1982).

[19]G. F. Chew and F. E. Low, Phys. Rev. 101, 1570 (1956).

[20]Y. Yamaguchi, Phys. Rev. 95, 1628 (1954); Y. Yamaguchi and Y. Yamaguchi, *ibid.* 95, 1635 (1954).